Supporting Information

Privileged Structures and Polypharmacology within and between Protein Families

*Joshua Meyers,[1] Nicola E. A. Chessum,[1] Salyha Ali,[1,2] N. Yi Mok,[1] Birgit Wilding,[1] A. Elisa Pasqua,[1] Martin Rowlands,[1] Michael J. Tucker,[1] Lindsay E. Evans,[1] Carl S. Rye,[1] Lisa O'Fee,[1] Yann-Vaï Le Bihan,[1,2] Rosemary Burke,[1] Michael Carter,[1] Paul Workman,[1] Julian Blagg,[1] Nathan Brown,[1] Rob L. M. van Montfort,[1,2] Keith Jones,[1] Matthew D. Cheeseman[1,]**

[1] Cancer Research UK Cancer Therapeutics Unit at The Institute of Cancer Research, London SW7 3RP, United Kingdom.

[2] Division of Structural Biology at The Institute of Cancer Research, London SW7 3RP, United Kingdom.

Nicola E. A. Chessum: 0000-0003-4125-320X
N. Yi Mok: 0000-0002-2827-3735
Birgit Wilding: 0000-0002-1896-3708
Yann-Vaï Le Bihan: 0000-0002-6850-9706
Rob L.M. van Montfort: 0000-0002-5688-3450
A. Elisa Pasqua: 0000-0002-7966-4672
Rosemary Burke: 0000-0002-0011-9701
Paul Workman: 0000-0003-1659-3034
Julian Blagg: 0000-0002-7409-0323
Nathan Brown: 0000-0001-9243-8699
Keith Jones: 0000-0002-9440-4094

Table of Contents:

Pocket Analysis

The *SiteHopper PatchScore* represents a summation of four Color and Shape Tanimoto coefficients weighted 3:1 in favor of Color similarity. Five pharmacophoric pseudocenter types make up the color forcefield: hydrogen bond donor, hydrogen bond acceptor, anion, cation and hydrophobe. Binding sites were identified with fpocket (version 2.0) which was implemented for ligand-independent cavity detection using default settings with two parameter alterations; the −r flag was set to 3.0 (default 4.5) and the −n flag was set to 3 (default 2). For each protein structure, chains were treated independently. For each chain, the cavity with the greatest fpocket Score was considered as the binding site – this was confirmed visually for binding sites pertinent to this analysis.

Table S1. CDK9 Pocket Analysis Dataset

Protein	*N (homology models)*	PDB IDs
CDK9	**21 (1)**	**3BLH, 3BLQ, 3BLR, 3LQ5, 3MI9, 3MIA, 3MY1, 3TN8, 3TNH, 3TNI, 4BCF, 4BCG, 4BCH, 4BCI, 4BCJ, 4EC8, 4EC9, 4IMY, 4OGR, 4OR5, *HM*(template:4IMY, identity:100%, source:SWISSMODEL)**
ERK5	4	2Q8Y, 4B99, 4IC7, 4IC8
PFPK5	4	1OB3, 1V0B, 1V0O, 1V0P
CDKL5	1	4BGQ
CDC2L5	1	5EFQ
CDK16	1	3MTL
CDK7	1	1UA2
CDK5	6	1H4L, 1UNG, 1UNH, 1UNL, 3O0G, 4AU8
CDK2 – structures taken from the sc-PDB database (2013)	180	1DI8, 1DM2, 1E1X, 1E9H, 1FVT, 1FVV, 1G5S, 1GIH, 1GIJ, 1H1Q, 1H1R, 1KE5, 1KE6, 1KE7, 1KE8, 1KE9, 1OI9, 1OIQ, 1OIT, 1OIY, 1P2A, 1P5E, 1PXM, 1PXN, 1PYE, 1R78, 1URW, 1W0X, 1W8C, 1Y8Y, 1Y91, 1YKR, 2A0C, 2B52, 2B53, 2B54, 2B55, 2BHE, 2BHH, 2BTR, 2BTS, 2C5N, 2C5V, 2C5X, 2C6I, 2C6K, 2C6L, 2C6T, 2CCI, 2DS1, 2DUV, 2FVD, 2I40, 2IW6, 2IW9, 2J9M, 2R3F, 2R3I, 2R3P, 2R64, 2UZB, 2UZD, 2UZE, 2UZL, 2UZN, 2UZO, 2VTI, 2VTJ, 2VTN, 2VTO, 2VTP, 2VTQ, 2VTS, 2VTT, 2VU3, 2VV9, 2W05, 2W06, 2W17, 2W1H, 2WEV, 2XMY, 2XNB, 3DDP, 3DDQ, 3DOG, 3EZR, 3EZV, 3FZ1, 3IG7, 3IGG, 3LE6, 3LFN, 3LFQ, 3LFS, 3NS9, 3PJ8, 3QQF, 3QQH, 3QQK, 3QQL, 3QRT, 3QTQ, 3QTR, 3QTS, 3QTU, 3QTW, 3QTX, 3QTZ, 3QU0, 3QWJ, 3QWK, 3QX2, 3QX4, 3QXO, 3QXP, 3QZH, 3QZI, 3R1Q, 3R28, 3R6X, 3R71, 3R7I, 3R7U, 3R7Y, 3R83, 3R8U, 3R8V, 3R8Z, 3R9D, 3R9H, 3R9N, 3R9O, 3RAH, 3RAI, 3RAK, 3RAL, 3RJC, 3RK5, 3RK7, 3RK9, 3RKB, 3RM6, 3RM7, 3RMF, 3RNI, 3RPO, 3RPR, 3RPV, 3RPY, 3S00, 3S0O, 3S1H, 3S2P, 3SQQ, 3SW4, 3SW7, 3TI1, 3TIZ, 3ULI, 3UNJ, 3UNK, 3WBL, 4ACM, 4BCO, 4BCP, 4BGH, 4EK4, 4EK6, 4EOI, 4EZ3, 4FKG, 4FKI, 4FKO, 4FKQ, 4FKS, 4FX3, 4I3Z, 4KD1, 4LYN
CDK4-cyclinD3	1	3G33
CDK4- cyclinD1	5(1)	2W96, 2W99, 2W9F, 2W9Z, *HM*(template:2W9Z, identity:99%, source:MODBASE)
PCTK3	3(3)	*HM*(template:1GZ8, identity:53%, source:MODBASE), *HM*(template:3PXR, identity:52%, source:MODBASE), *HM*(template:3COI, identity:36%, source:NYSGXRC)
CDK14	3(3)	*HM*(template:3MTL, identity:60%, source:MODBASE), *HM*(template:3O0G, identity:54%, source:SWISSMODEL), *HM*(template:3MTL, identity:56%, source:SWISSMODEL)
TLK1	3(3)	*HM* (template:4EJN, identity:39%, source:MODBASE), *HM*(template:4CFE, identity:37%, source:SWISSMODEL), *HM*(template:2HAK, identity:37%, source:SWISSMODEL)
TLK2	3(3)	*HM* (template:2BAJ, identity:41%, source:MODBASE), *HM*(template:3ORZ, identity:33%, source:SWISSMODEL), *HM*(template:2HAK, identity:37%, source:SWISSMODEL)
ICK	3(3)	*HM* (template:3GBZ, identity:43%, source:MODBASE), *HM*(template:4AWI, identity:31%, source:SWISSMODEL), *HM*(template:4Y72, identity:42%, source:SWISSMODEL)
ERK8	3(3)	*HM* (template:3DLS, identity:32%, source:MODBASE), *HM*(template:3OZ6, identity:50%, source:MODBASE), *HM*(template:3OZ6, identity:49%, source:SWISSMODEL)
GSK3A	2(2)	*HM* (template:1J1B, identity:86%, source:MODBASE), *HM*(template:4ACC, identity:86%, source:SWISSMODEL)
TAOK1	2(2)	*HM* (template:1U5Q, identity:89%, source:MODBASE), *HM*(template:1U5Q, identity:89%, source:SWISSMODEL)
HIPK2	3(3)	*HM* (template:3ANQ, identity:42%, source:MODBASE), *HM*(template:3KVW, identity:35%, source:SWISSMODEL), *HM*(template:4MQ2, identity:40%, source:SWISSMODEL)
HIPK3	3(3)	*HM* (template:3ANQ, identity:42%, source:MODBASE), *HM*(template:3O7L, identity:38%, source:SWISSMODEL), *HM*(template:4MQ2, identity:40%, source:SWISSMODEL)
Total	**252**	

Table S2. Results of *SiteHopper* Pocket Analysis:

Rank	Kinase	*N pockets*	Max SiteHopper PatchScore (CDK9)	CDK9 code	Kinase code
1	CDK9	33	2.66 (excluding self)	4BCI	4BCH
2	CDK2	180	1.86	3LQ5	2C5V
3	TAOK1	2	1.81	3BLR	*HM* (template:1U5Q, identity:89%, source:MODBASE),
4	CDC2L5	3	1.58	3BLQ	5EFQ
5	CDK14	4	1.58	3BLR	*HM*(template:3O0G, identity:54%, source:SWISSMODEL)
6	HIPK2	4	1.48	3MY1	*HM*(template:3KVW, identity:35%, source:SWISSMODEL)
7	CDKL5	1	1.47	3BLR	4BGQ
8	HIPK3	3	1.42	3BLR	*HM* (template:3ANQ, identity:42%, source:MODBASE)
9	ICK	4	1.38	4EC8	*HM*(template:4Y72, identity:42%, source:SWISSMODEL)
10	PFPK5	5	1.35	3BLR	1V0P
11	CDK4-cyclinD1	6	1.31	3BLR	*HM*(template:2W9Z, identity:99%, source:MODBASE)

B-Raf Docking Study

An enzyme-inhibitor cocrystal structure of human B-Raf kinase with a bisamide chemotype (PDB 4G9C) [1] was prepared for modeling using Protein Preparation Wizard in Maestro.[2] To propose predicted binding modes of ligands, Glide (Grid-based Ligand Docking with Energetics) [3] was used for the docking experiments. The receptor grid was defined by a grid box of 30 × 30 × 30 $Å^3$ with a default inner box (10 × 10 × 10 $Å^3$) centered on the cocrystallized ligand in PDB 4G9C.

The dual pirin/B-Raf ligand compound **2** was prepared using LigPrep,[4] applying the OPLS_2005 force field with possible tautomeric and ionization states within pH range 5.0−9.0 generated. Using Glide Extra Precision (XP) settings, flexible docking of the ligand was conducted without any constraints. The docked pose with the lowest RMSD to the bisamide-containing aromatic ring of the crystallized ligand in PDB 4G9C was selected as the predicted binding pose.

[1] Wenglowsky *et al.* (**2012**) *Bioorg. Med. Chem. Lett.*, *22*, 6237.
[2] Maestro version 11; Schrödinger, LLC: New York, NY, 2017.
[3] Glide, version 7.5; Schrödinger, LLC: New York, NY, 2017.
[4] LigPrep, version 2.5; Schrödinger, LLC: New York, NY, 2011.

References for the Activity of Reported B-Raf Inhibitors

PLX4720: Tsai, J.; Lee, J. T.; Wang, W.; Zhang, J.; Cho, H.; Mamo, S.; Bremer, R.; Gillette, S.; Kong, J.; Haass, N. K.; Sproesser, K.; Li, L.; Smalley, K. S. M.; Fong, D.; Zhu, Y.; Marimuthu, A.; Nguyen, H.; Lam, B.; Liu, J.; Cheung, I.; Rice, J.; Suzuki, Y.; Luu, C.; Settachatgul, C.; Shellooe, R.; Cantwell, J.; Kim, S.; Schlessinger, J.; Zhang, K. Y. J.; West, B. L.; Powell, B.; Habets, G.; Zhang, C.; Ibrahim, P. N.; Hirth, P.; Artis, D. R.; Herlyn, M., Bollag, G. Discovery of a selective inhibitor of oncogenic B-Raf kinase with potent antimelanoma activity. *Proc. Natl. Acad. Sci. U. S. A.* **2008**, *105*, 3041-3046.

Vemurafenib: Bollag, G.; Hirth, P.; Tsai, J.; Zhang, J.; Ibrahim, P. N.; Cho, H.; Spevak, W.; Zhang, C.; Zhang, Y.; Habets, G.; Burton, E. A.; Wong, B.; Tsang, G.; West, B. L.; Powell, B.; Shellooe, R.; Marimuthu, A.; Nguyen, H.; Zhang, K. Y. J.; Artis, D. R.; Schlessinger, J.; Su, F.; Higgins, B.; Iyer, R.; D'Andrea, K.; Koehler, A.; Stumm, M.;

Lin, P. S.; Lee, R. J.; Grippo, J.; Puzanov, I.; Kim, K. B.; Ribas, A.; McArthur, G. A.; Sosman, J. A.; Chapman, P. B.; Flaherty, K. T.; Xu, X.; Nathanson, K. L.; Nolop, K. Clinical efficacy of a RAF inhibitor needs broad target blockade in BRAF-mutant melanoma *Nature* **2010**, *467*, 596-599.

AZ268: Wenglowsky, S.; Ren, L.; Grina, J.; Hansen, J. D.; Laird, E. R.; Moreno, D.; Dinkel, V.; Gloor, S. L.; Hastings, G.; Rana, S.; Rasor, K.; Sturgis, H. L.; Voegtli, W. C.; Vigers, G.; Willis, B.; Mathieu, S.; Rudolph, J. Highly potent and selective 3-N-methylquinazoline-4(3H)-one based inhibitors of B-RafV600E kinase. *Bioorg. Med. Chem. Lett.* **2014**, *24*, 1923-1927.

TAK-632: Okaniwa, M.; Hirose, M.; Arita, T.; Yabuki, M.; Nakamura, A.; Takagi, T.; Kawamoto, T.; Uchiyama, N.; Sumita, A.; Tsutsumi, S.; Tottori, T.; Inui, Y.; Sang, B.; Yano, J.; Aertgeerts, K.; Yoshida, S.; Ishikawa, T. Discovery of a selective kinase inhibitor (TAK-632) targeting pan-RAF inhibition: design, synthesis, and biological evaluation of C7-substituted 1,3-benzothiazole derivatives. *J. Med. Chem.* **2013**, *56*, 6478-6494.

RAF265: Williams, T. E.; Subramanian, S.; Verhagen, J.; McBride, C. M.; Costales, A.; Sung, L.; Antonios-McCrea, W.; McKenna, M.; Louie, A. K.; Ramurthy, S.; Levine, B.; Shafer, C. M.; Machajewski, T.; Renhowe, P. A.; Appleton, B. A.; Amiri, P.; Chou, J.; Stuart, D.; Aardalen, K.; Poon, D. *ACS Med. Chem. Lett.* **2015**, *6*, 961-965.

Dabrafenib: Rheault, T. R.; Stellwagen, J. C.; Adjabeng, G. M.; Hornberger, K. R.; Petrov, K. G.; Waterson, A. G.; Dickerson, S. H.; Mook, Jr., R. A.; Laquerre, S. G.; King, A. J.; Rossanese, O. W.; Arnone, M. R.; Smitheman, K. N.; Kane-Carson, L. S.; Han, C.; Moorthy, G. S.; Moss, K. G.; Uehling, D. E. Discovery of Dabrafenib: A selective inhibitor of raf kinases with antitumor activity against B‑Raf-driven tumors. *ACS Med. Chem. Lett.* **2013**, *4*, 358-362.

GDC-0879: Hansen, J. D.; Grina, J.; Newhouse, B.; Welch, M.; Topalov, G.; Littman, N.; Callejo, M.; Gloor, S.; Martinson, M.; Laird, E.; Brandhuber, B. J.; Vigers, G.; Morales, T.; Woessner, R.; Randolph, N.; Lyssikatos, J.; Olivero, A. *Bioorg. Med. Chem. Lett.* **2008**, *18*, 4692-4695.

Chemistry Experimental

All final compounds were screened through our in-house computational PAINS filter and gave no structural alerts as potential assay interference compounds. Unless otherwise stated, reactions were conducted in oven dried glassware under an atmosphere of nitrogen or argon using anhydrous solvents. All commercially obtained reagents and solvents were used as received. Thin layer chromatography (TLC) was performed on pre-coated aluminum sheets of silica (60 F254 nm, Merck) and visualized using short-wave UV light. Flash column chromatography was carried out on Merck silica gel 60 (particle size 40-65 μm). Column chromatography was also performed on Biotage SP1 or Isolera 4 purification systems using Biotage Flash silica cartridges (SNAP KP-Sil). Ion exchange chromatography was performed using acidic Biotage Isolute Flash SCX-2 columns.

Semi-preparative HPLC: 500 uL standard injections (with needle wash) of the sample were made on a Phenomenex Gemini C18 column (5μ, 250x21.2 mm, Phenomenex, Torrence, USA). Chromatographic separation at room temperature was carried out using a 1200 Series Preparative HPLC (Agilent, USA) over a 15 minutes gradient elution from 90:10 to 0:100 water:methanol (both modified with 0.1% formic acid) at a flow rate of 20 mL/min. UV-Vis spectra were acquired at 254 nm on a 1200 Series Prep Scale diode array detector (Agilent). Post-UV and pre-MS splitting was achieved using an Active Split (Agilent) before being infused into a 6120 Series Quad mass spectrometer fitted with an ESI/APCI Multimode ionization source (Agilent). Collection was triggered by UV signal and collected

on a 1200 Series Fraction Collector (Agilent). ^{1}H-NMR spectra were recorded on Bruker Avance 500 (500 MHz) spectrometers using an internal deuterium lock. Chemical shifts are quoted in parts per million (ppm) using the following internal references: $CDCl_3$ (δH 7.26), MeOD (δH 3.31) and DMSO-d_6 (δH 2.50). Signal multiplicities are recorded as singlet (s), doublet (d), triplet (t), quartet (q), quintet (qn), and multiplet (m), doublet of doublets (dd), doublet of doublet of doublets (ddd), broad (br), obscured (obs) or apparent (app). Coupling constants, *J*, are measured to the nearest 0.1 Hz. ^{13}C-NMR spectra were recorded on Bruker Avance 500 spectrometers at 126 MHz using an internal deuterium lock. Chemical shifts are quoted to 0.01 ppm, unless greater accuracy was required, using the following internal references: $CDCl_3$ (δC 77.0), MeOD (δC 49.0) and DMSO-d_6 (δC 39.5). High resolution mass spectra were recorded on an Agilent 1200 series HPLC and diode array detector coupled to a 6210 time of flight mass spectrometer with dual multimode APCI/ESI source (Methods I-IV) or on a Waters Acquity UPLC and diode array detector coupled to a Waters G2 QToF mass spectrometer fitted with a multimode ESI/APCI source.

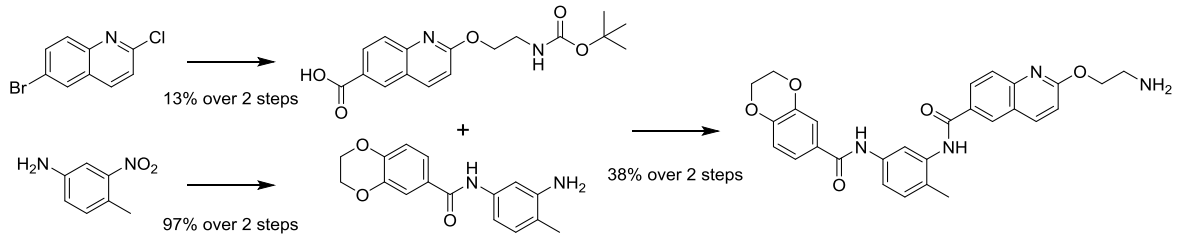

For details of Steps (i) to (vi) see: Cheeseman, M. D.; Chessum, N. E.; Rye, C. S.; Pasqua, A. E.; Tucker, M. J.; Wilding, B.; Evans, L. E.; Lepri, S.; Richards, M.; Sharp, S. Y.; Ali, S.; Rowlands, M.; O'Fee, L.; Miah, A.; Hayes, A.; Henley, A. T.; Powers, M.; Te Poele, R.; De Billy, E.; Pellegrino, L.; Raynaud, F.; Burke, R.; van Montfort, R. L.; Eccles, S. A.; Workman, P.; Jones, K. *J. Med. Chem.* **2017**, *60*, 180-201.

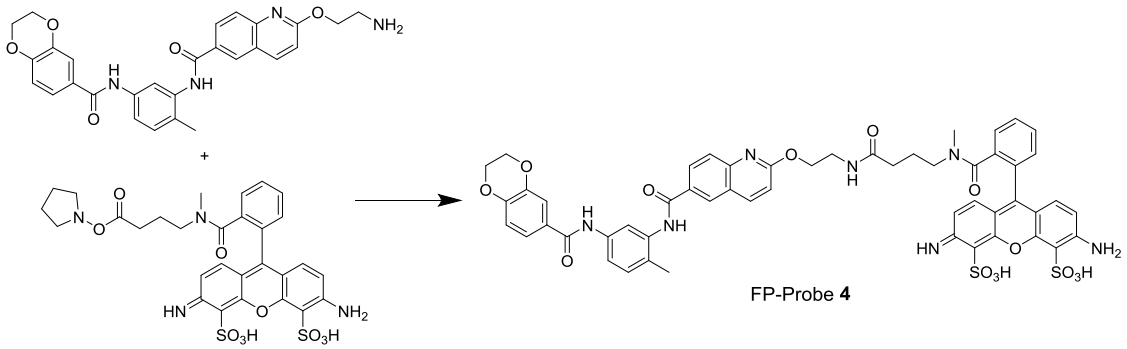

6-amino-9-(2-((4-((2-((6-((5-(2,3-dihydrobenzo[*b*][1,4]dioxine-6-carboxamido)-2-methylphenyl)carbamoyl)quinolin-2-yl)oxy)ethyl)amino)-4-oxobutyl)(methyl)carbamoyl)phenyl)-3-imino-3*H*-xanthene-4,5-disulfonic acid **4**

To a solution of 2-(2-aminoethoxy)-*N*-(5-(2,3-dihydrobenzo[*b*][1,4]dioxine-6-carboxamido)-2-methylphenyl)quinoline-6-carboxamide (1.0 mg, 2.0 μmol) in dry DMF (0.18 mL) in the dark was added 6-amino-3-imino-9-(2-(methyl(4-oxo-4-(pyrrolidin-1-yloxy)butyl)carbamoyl)phenyl)-3*H*-xanthene-4,5-disulfonic acid (1.5 mg, 2.2 μmol).and $^{i}Pr_2NEt$ (drop) and the mixture was stirred overnight. After this time, the solvent was removed under reduced pressure and the resulting residue was purified by semi-prep chromatographic separation. Semi-prep HPLC as carried out at room temperature using a Gilson GX-281 Liquid Handler system combined with a Gilson 322 HPLC pump (Gilson, Middleton, USA) over a 15 minute gradient elution (Grad15mins20mls.m) from 10:90 to 100:0 methanol:water (both modified with 0.1% formic acid) at a flow rate of 20 mL/min. UV-Vis spectra were acquired at

254 nm on a Gilson 156 UV-Vis detector (Gilson, Middleton, USA). Collection was triggered by UV signal, and collected using a Gilson GX-281 Liquid Handler system (Gilson, Middleton, USA), to give the title compound **4** as an orange oil in 25% yield HRMS (ESI) $C_{53}H_{48}N_7O_{14}S_2$ $(M+H)^+$ requires 1070.2695, found 1070.2748.

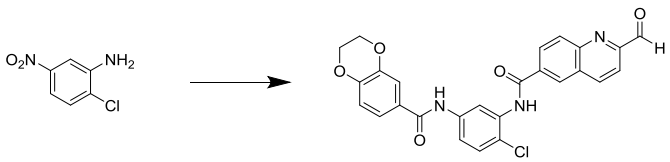

N-(2-chloro-5-(2,3-dihydrobenzo[*b*][1,4]dioxine-6-carboxamido)phenyl)-2-formylquinoline-6-carboxamide

For the synthesis of the chlorobisamide aldehyde intermediate see: Chessum, N. E. A.; Sharp, S. Y.; Caldwell, J. J.; Pasqua, A. E.; Wilding, B.; Colombano, G.; Collins, I.; Ozer, B.; Richards, M.; Rowlands, M.; Stubbs, M.; Burke, R.; McAndrew, P. C.; Clarke, P. A.; Workman, P.; Cheeseman, M. D.; Jones, K. *J. Med.Chem.* **2018**, *61*, 918-933.

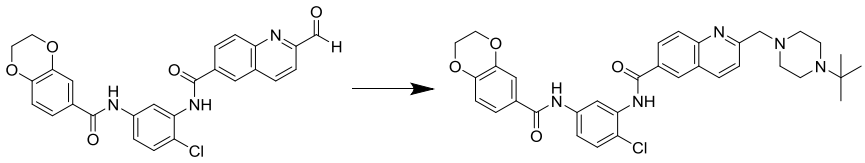

2-((4-(tert-butyl)piperazin-1-yl)methyl)-*N*-(2-chloro-5-(2,3-dihydrobenzo[*b*][1,4]dioxine-6-carboxamido)phenyl)quinoline-6-carboxamide **8**

To a solution of *N*-(2-chloro-5-(2,3-dihydrobenzo[*b*][1,4]dioxine-6-carboxamido)phenyl)-2-formylquinoline-6-carboxamide (300 mg, 0.62 mmol) in CH_2Cl_2/MeOH (5 mL, 5:1) was added 1 1-(tert-butyl)piperazine (260 mg, 1.9 mM) and the mixture was stirred at room temperature for 12 hours. After this time, $NaBH(OAc_3)_3$ was added and the mixture for 2 h, then quenched with sat. $NaHCO_3$ solution, extracted with CH_2Cl_2/MeOH (9:1), dried and the solvent removed under reduced pressure. The resulting residue was purified by silica gel chromatography, eluting with a 10% CH_2Cl_2:MeOH gradient to give the desired product (60 mg, 16%) as a beige solid. 1H NMR (500 MHz, DMSO-d6) δ ^{1}H NMR (500 MHz, DMSO-d_6) δ 10.34 (s, 1H), 10.29 (s, 1H), 8.66 (d, *J*=1.89 Hz, 1H), 8.49 (d, *J*=8.51 Hz, 1H), 8.26 (dd, *J*=2.21, 8.83 Hz, 1H), 8.14 (d, *J*=2.52 Hz, 1H), 8.09 (d, *J*=8.83 Hz, 1H), 7.69-7.80 (m, 2H), 7.49-7.61 (m, 3H), 7.00 (d, *J*=8.20 Hz, 1H), 4.28-4.36 (m, 4H), 3.79 (s, 2H), 1.03 (br s, 9H). 13C NMR (126 MHz, DMSO-d6) δ ^{13}C NMR (126 MHz, DMSO-d_6) δ 165.5, 165.1, 162.2, 148.7, 147.0, 143.4, 139.1, 138.0, 135.4, 131.8, 129.8, 129.3, 128.9, 128.4, 127.8, 126.7, 124.1, 122.3, 121.8, 120.3, 119.7, 117.4, 117.2, 65.4, 64.9, 64.5, 54.2, 45.8, 26.0. HRMS (ESI+): calcd for $C_{34}H_{37}Cl^{35}N_5O_4$ $(M + H)^+$, 614.2534; found 614.2530.

Pirin Fluorescence Polarization Assay

General Information: Unless otherwise stated, the assay buffer contained 50 mM HEPES pH 7.4, 150 mM NaCl, 0.1% (w/w) CHAPS, 2% DMSO and the assay was conducted in 384 Plus F ProxiPlates (PerkinElmer). Plates were centrifuged at 1000 rpm for 1 minute prior to incubation and read using a 2103 Envision Multilabel Plate Reader. Excitation and emission wavelengths used for green probes were 480 nm and 535 nm, respectively. Fluorescence polarization was measured in units of millipolarization (mP) and all experiments were performed in triplicate.

Determination of optimal probe concentration: 5 µL of pirin (400nM in assay buffer) or 5 µL assay buffer and increasing concentrations of probe (5 µL, dilution series from 0.2 up to 1000nM) were added. From the plotted data, a probe concentration of 2 nM was selected and gave an assay window of 4.0 with a Z' of 0.74.

Fluorescent probe K_D determination: 5 µL of probe molecule (4 nM in assay buffer) to increasing concentrations of the pirin protein (5 µL, dilution series from 0.2 to 200 nM). Fluorescence polarization values for tracer control wells (2 nM probe in assay buffer only) were subtracted from each data point prior to data analysis. The K_D determination was analyzed using non-linear regression analysis (one site–specific binding model, GraphPad Prism 6) and gave a K_D of 12 nM.

Compound IC_{50} determination: Compounds (0.2 µL at 50 x screening concentration in DMSO) were dispensed using an ECHO 550 Liquid Handler (Labcyte Inc.). To the corresponding wells, 5 µL of probe molecule (4 nM in assay buffer) and 5 µL of pirin protein (60 nM) were added. Tracer controls (2 nM probe molecule only) and bound tracer controls (2 nM probe in the presence of appropriate protein concentration) were included on each assay plate. IC_{50} determination was performed using non-linear least squares curve fitting (GraphPad Prism 6, log(inhibitor) vs. response-variable slope (four parameters)).

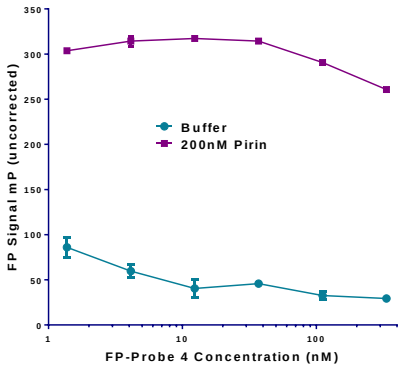

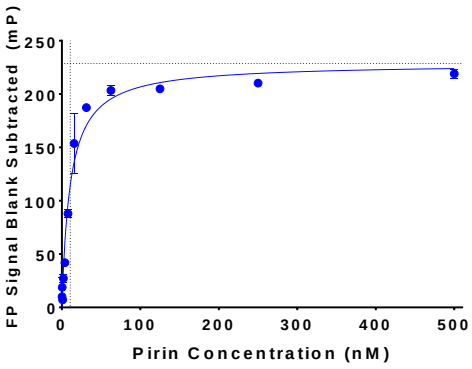

One site -- Specific binding	
Best-fit values	
Bmax	228.7
Kd	10.65
Std. Error	
Bmax	6.676
Kd	1.368
95% CI (profile likelihood)	
Bmax	215.5 to 242.3
Kd	8.31 to 13.59
Goodness of Fit	
Degrees of Freedom	22
R square	0.9713
Absolute Sum of Squares	5119
Sy.x	15.25
Number of points	
# of X values	24
# Y values analyzed	24

Figure S1. Pirin FP-Probe Binding Data

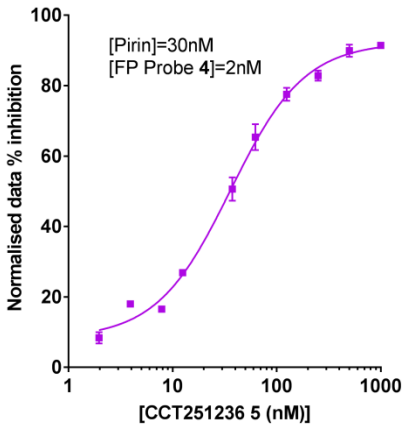

[Inhibitor] vs. response -- Variable slope (four parameters)	
Best-fit values	
Bottom	8.253
Top	92.33
HillSlope	-1.223
IC50	35.99
logIC50	1.556
Span	84.08
Std. Error	
Bottom	2.641
Top	2.108
HillSlope	0.1363
IC50	3.258
Span	4.04
95% CI (profile likelihood)	
Bottom	1.289 to 13.26
Top	88.19 to 97.73
HillSlope	-1.565 to -0.9432
IC50	29.35 to 43.27
logIC50	1.468 to 1.636
Goodness of Fit	
Degrees of Freedom	16
R square	0.9917
Absolute Sum of Squares	161.2
Sy.x	3.174
Constraints	
IC50	IC50 > 0
Number of points	
# of X values	20
# Y values analyzed	20

Figure S2. Example Pirin FP-probe Displacement Data

Pirin FP-Probe Binding Analysis

Huang's equation was used to calculate K_i values from the measured IC_{50}s. See equation below:

$$IC_{50} = \left(\frac{f_0 K_d}{(1-f_0)(2-f_0)} + \frac{f_0 L_0}{2} \right) \left(\frac{K_i (2-f_0)}{K_d f_0} + 1 \right)$$

The equation states that the IC_{50} for a ligand that is competitive for binding with the assay probe is related to the binding affinity of the ligand (K_i), the bound fraction of the probe (f_0), the binding affinity of the probe (K_d) and the concentration of the probe (L_0). For competition experiments, it is recommended that a protein concentration giving a bound fraction between 0.5 and 0.8 be selected. A bound fraction below 0.7 will often result in an assay that is not statistically robust due to the decreased size of the binding window, however as the bound fraction approaches 1 the relationship between K_i and IC_{50} deviates from linear and the resolvable range of the assay decreases. For these reasons, a bound fraction of 0.72 was used for all assays.

$$R_0 = \frac{K_d f_0}{1 - f_o} + f_0 L_0$$

Where R_0=[protein]

When K_d=11 nM, F_b=0.72 and L_0=2 nM

R_0=30 nM

All IC_{50} values within 2-fold of the protein concentration were considered tight-binding.

For details see Huang, X. *J. Biomol. Screen.* **2003** *8*, 34-38.

Pirin and B-Raf Crystallography Analysis

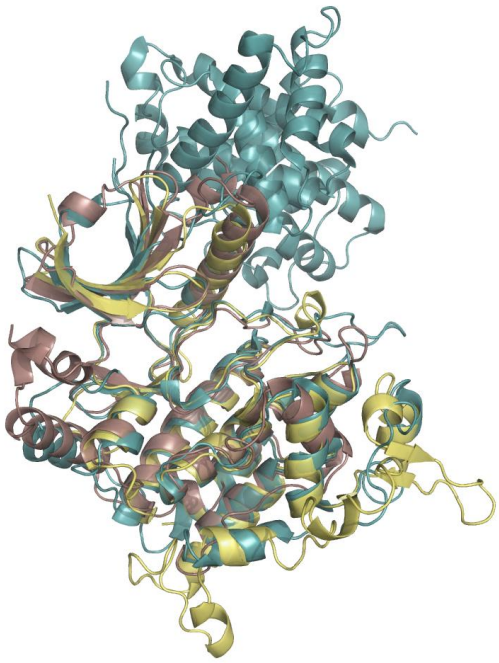

Figure S3. Overlay of CDK9 (PDB: 4EC8, turquoise) and homology models of TAOK1 (brown) and HIPK2 (yellow)

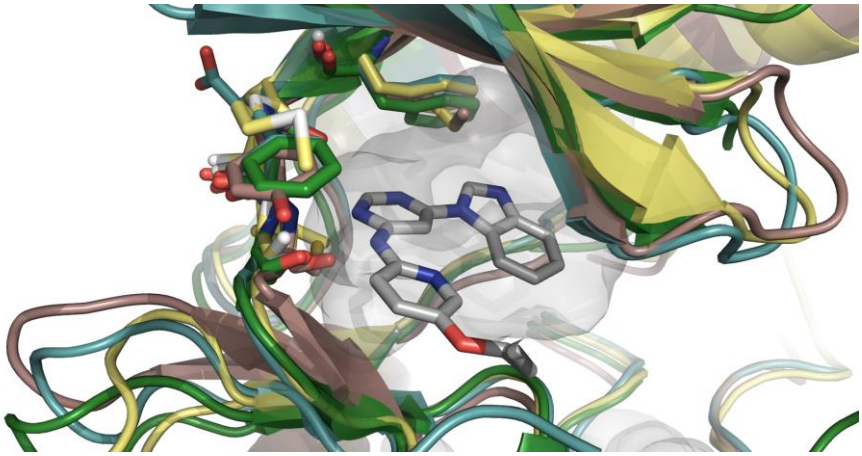

Figure S4. Key Residues Leading to the Intra-Family Polypharmacology as Detected by the *SiteHopper* Pocket Analysis. CDK9 (PDB: 4EC8, turquoise), CDK2 (PDB: 4BZD, green) and homology models of TAOK1 (brown) and HIPK2 (yellow).

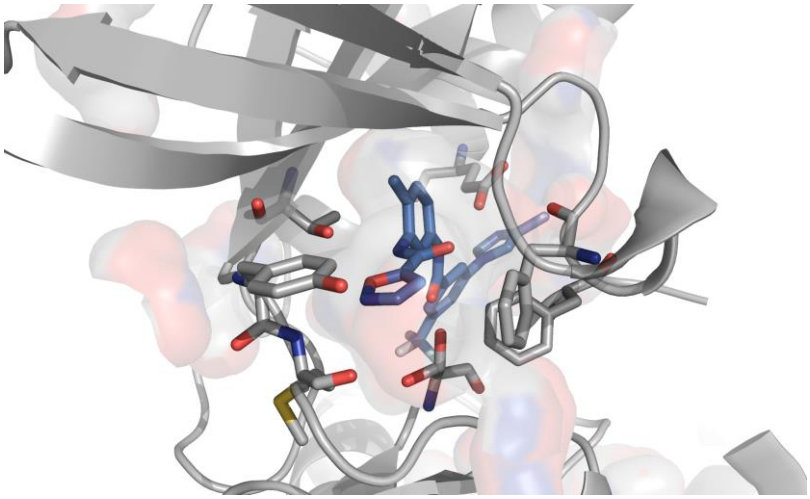

Figure S5. Crystal structures of the bisamide chemotype bound to EphA3 (PDB: 3DZQ).

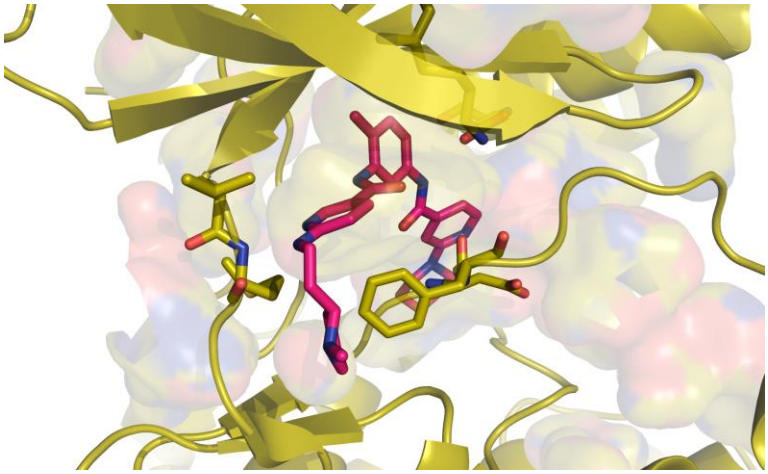

Figure S6. Crystal structures of the bisamide chemotype bound to p38 (PDB: 3KQ7).

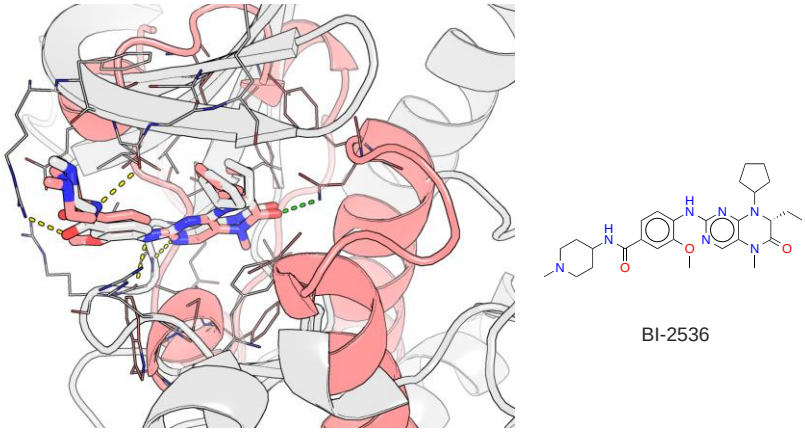

Figure S7. Overlay of the binding site of BRD4 (PDB: 4OGI, salmon) with PLK1 (PDB ID: 2RKU, white), using the bound ligand, BI-2536.

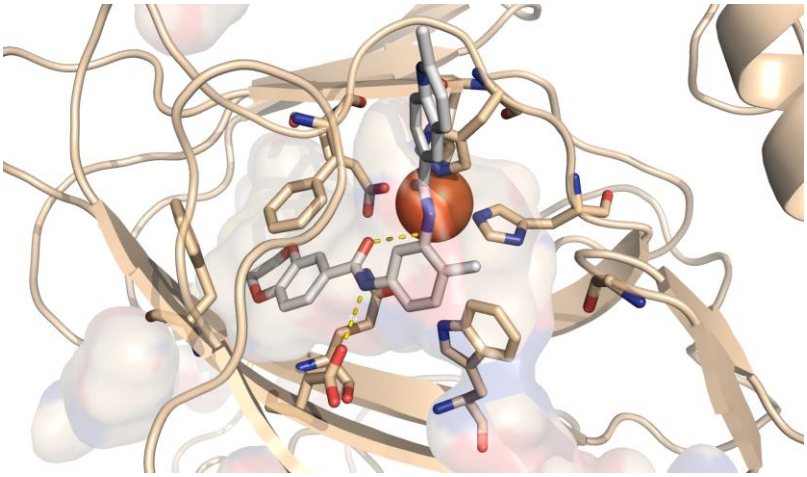

Figure S8. Structure of Bisamide 2 bound to Pirin highlighting key residues.

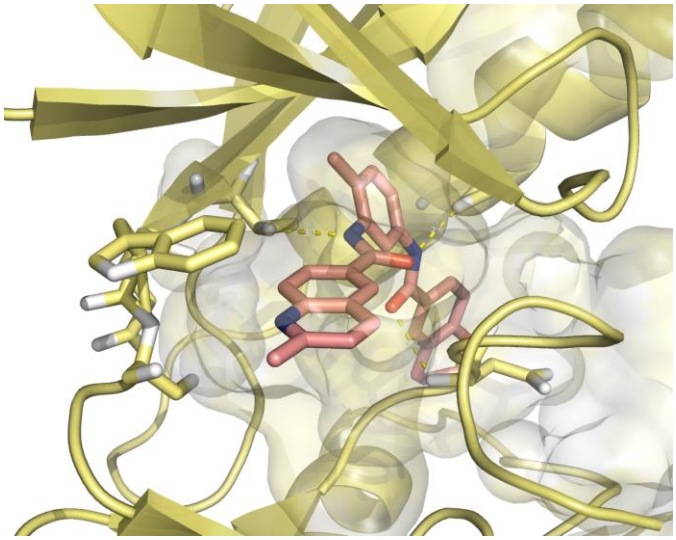

Figure S9. Docking Pose of Bisamide 2 Bound to B-Raf

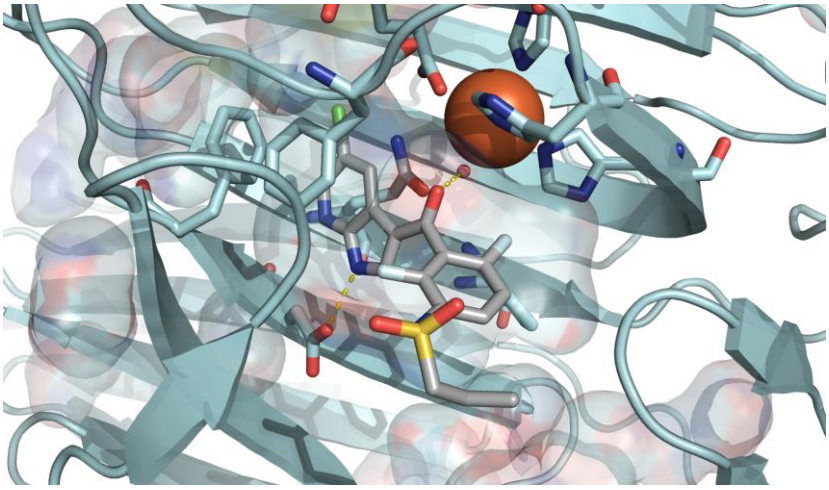

Figure S10. Structure of PLX4720 7 bound to Pirin highlighting key residues. NB: the sulfonamide moiety could not be observed in the electron density due to its flexibility but is shown here in one possible conformation for clarity.

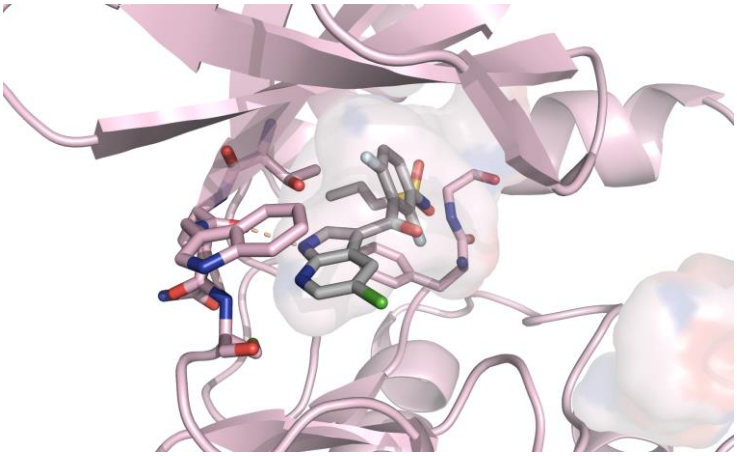

Figure S11. Structure of PLX4720 7 bound to B-Raf highlighting key residues.

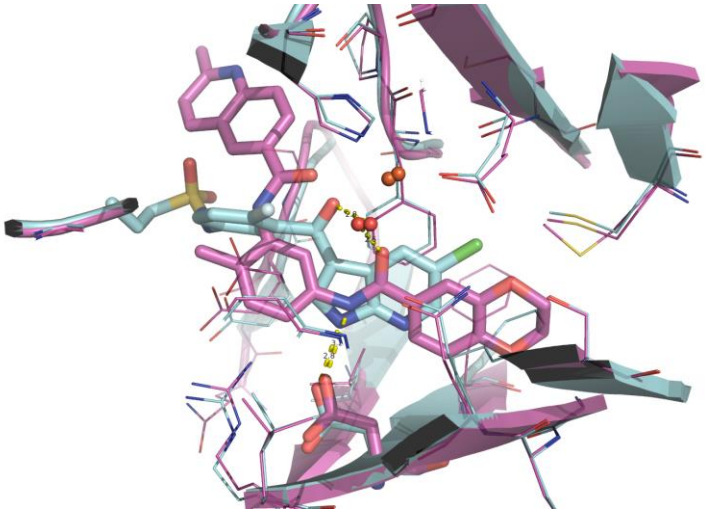

Figure S12. Overlay of bisamide 2 (purple) and PLX4720 7 bound to pirin.

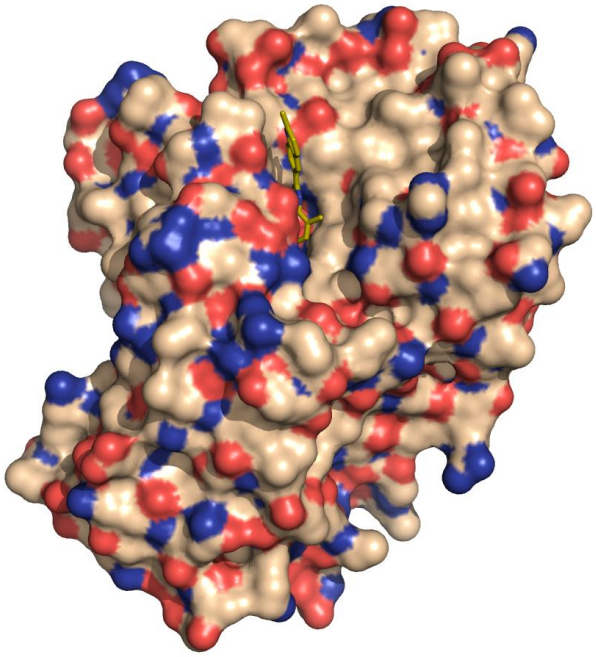

Figure S13. FP-Assay Probe Design. Surface representation of Pirin with Bisamide 2 (gold) bound. The methylene quinoline group is clearly solvent exposed.

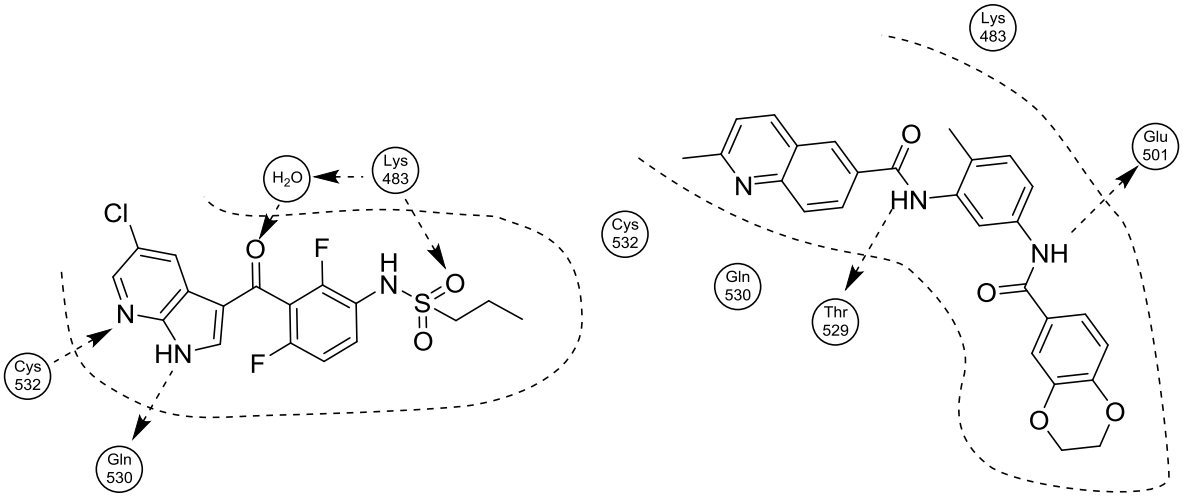

Figure S14. Analysis of key interactions in B-Raf

Kinase Assay Data

Table S3. B-Raf Assay Data

Life Technologies' SelectScreen® Profiling Service: 10-point Titration Results

SSBK-Z'-LYTE (Paisley UK)

% Phosphorylation	Pass
Z' Determination	Pass

Project #	Compound Name	Kinase Tested	[ATP] Tested (µM)	IC50 (nM)	Hillslope	R^2 Value	Conc of Compound (nM)	%Inhibition Point 1	%Inhibition Point 2	Development Reaction Interference	Test Compound Interference Coumarin	Test Compound Interference Fluorescein	Z'	Kinase Part# / Lot#	Graph
SSBK9431_23647	CCT245232	BRAF	100	415	0.59	0.9853	50000	91	94	Pass	Pass	Pass	0.55	PV3848/34486	BRAF : ATP [100] CCT245232
SSBK9431_23647	CCT245232	BRAF	100	415	0.59	0.9853	16700	82	94	Pass	Pass	Pass	0.55	PV3848/34486	
SSBK9431_23647	CCT245232	BRAF	100	415	0.59	0.9853	5560	82	81	Pass	Pass	Pass	0.55	PV3848/34486	
SSBK9431_23647	CCT245232	BRAF	100	415	0.59	0.9853	1850	62	79	Pass	Pass	Pass	0.55	PV3848/34486	
SSBK9431_23647	CCT245232	BRAF	100	415	0.59	0.9853	617	41	54	Pass	Pass	Pass	0.55	PV3848/34486	
SSBK9431_23647	CCT245232	BRAF	100	415	0.59	0.9853	206	40	30	Pass	Pass	Pass	0.55	PV3848/34486	
SSBK9431_23647	CCT245232	BRAF	100	415	0.59	0.9853	69.0	9	21	Pass	Pass	Pass	0.55	PV3848/34486	
SSBK9431_23647	CCT245232	BRAF	100	415	0.59	0.9853	23.0	19	15	Pass	Pass	Pass	0.55	PV3848/34486	
SSBK9431_23647	CCT245232	BRAF	100	415	0.59	0.9853	7.70	-19	5	Pass	Pass	Pass	0.55	PV3848/34486	
SSBK9431_23647	CCT245232	BRAF	100	415	0.59	0.9853	2.57	6	-12	Pass	Pass	Pass	0.55	PV3848/34486	
SSBK9431_23647	CCT245232	BRAF V599E	100	209	1.16	0.9924	50000	96	94	Pass	Pass	Pass	0.63	PV3849/274067	BRAF V599E : ATP [100] CCT245232
SSBK9431_23647	CCT245232	BRAF V599E	100	209	1.16	0.9924	16700	92	89	Pass	Pass	Pass	0.63	PV3849/274067	
SSBK9431_23647	CCT245232	BRAF V599E	100	209	1.16	0.9924	5560	92	90	Pass	Pass	Pass	0.63	PV3849/274067	
SSBK9431_23647	CCT245232	BRAF V599E	100	209	1.16	0.9924	1850	81	82	Pass	Pass	Pass	0.63	PV3849/274067	
SSBK9431_23647	CCT245232	BRAF V599E	100	209	1.16	0.9924	617	78	80	Pass	Pass	Pass	0.63	PV3849/274067	
SSBK9431_23647	CCT245232	BRAF V599E	100	209	1.16	0.9924	206	48	53	Pass	Pass	Pass	0.63	PV3849/274067	
SSBK9431_23647	CCT245232	BRAF V599E	100	209	1.16	0.9924	69.0	26	33	Pass	Pass	Pass	0.63	PV3849/274067	
SSBK9431_23647	CCT245232	BRAF V599E	100	209	1.16	0.9924	23.0	17	27	Pass	Pass	Pass	0.63	PV3849/274067	
SSBK9431_23647	CCT245232	BRAF V599E	100	209	1.16	0.9924	7.70	9	14	Pass	Pass	Pass	0.63	PV3849/274067	
SSBK9431_23647	CCT245232	BRAF V599E	100	209	1.16	0.9924	2.57	15	14	Pass	Pass	Pass	0.63	PV3849/274067	
SSBK11477_31239	CCT251236-08	BRAF	100	2930	0.73	0.9346	10000	58	65	Pass	Pass	Pass	0.76	PV3848/1113215	BRAF : ATP [100] CCT251236-08
SSBK11477_31239	CCT251236-08	BRAF	100	2930	0.73	0.9346	3330	67	43	Pass	Pass	Pass	0.76	PV3848/1113215	
SSBK11477_31239	CCT251236-08	BRAF	100	2930	0.73	0.9346	1110	23	25	Pass	Pass	Pass	0.76	PV3848/1113215	
SSBK11477_31239	CCT251236-08	BRAF	100	2930	0.73	0.9346	370	11	25	Pass	Pass	Pass	0.76	PV3848/1113215	
SSBK11477_31239	CCT251236-08	BRAF	100	2930	0.73	0.9346	123	-21	1	Pass	Pass	Pass	0.76	PV3848/1113215	
SSBK11477_31239	CCT251236-08	BRAF	100	2930	0.73	0.9346	41.2	-9	-8	Pass	Pass	Pass	0.76	PV3848/1113215	
SSBK11477_31239	CCT251236-08	BRAF	100	2930	0.73	0.9346	13.7	-8	-13	Pass	Pass	Pass	0.76	PV3848/1113215	
SSBK11477_31239	CCT251236-08	BRAF	100	2930	0.73	0.9346	4.57	-22	12	Pass	Pass	Pass	0.76	PV3848/1113215	
SSBK11477_31239	CCT251236-08	BRAF	100	2930	0.73	0.9346	1.52	-7	-23	Pass	Pass	Pass	0.76	PV3848/1113215	
SSBK11477_31239	CCT251236-08	BRAF	100	2930	0.73	0.9346	0.508	6	-3	Pass	Pass	Pass	0.76	PV3848/1113215	
SSBK11477_31239	CCT363294-01	BRAF	100	>10000	1.06	0.6332	10000	15	32	Pass	Pass	Pass	0.76	PV3848/1113215	BRAF : ATP [100] CCT363294-01
SSBK11477_31239	CCT363294-01	BRAF	100	>10000	1.06	0.6332	3330	6	-3	Pass	Pass	Pass	0.76	PV3848/1113215	
SSBK11477_31239	CCT363294-01	BRAF	100	>10000	1.06	0.6332	1110	-4	-8	Pass	Pass	Pass	0.76	PV3848/1113215	
SSBK11477_31239	CCT363294-01	BRAF	100	>10000	1.06	0.6332	370	-26	-12	Pass	Pass	Pass	0.76	PV3848/1113215	
SSBK11477_31239	CCT363294-01	BRAF	100	>10000	1.06	0.6332	123	-22	-28	Pass	Pass	Pass	0.76	PV3848/1113215	
SSBK11477_31239	CCT363294-01	BRAF	100	>10000	1.06	0.6332	41.2	-36	-33	Pass	Pass	Pass	0.76	PV3848/1113215	
SSBK11477_31239	CCT363294-01	BRAF	100	>10000	1.06	0.6332	13.7	-17	-16	Pass	Pass	Pass	0.76	PV3848/1113215	
SSBK11477_31239	CCT363294-01	BRAF	100	>10000	1.06	0.6332	4.57	-27	9	Pass	Pass	Pass	0.76	PV3848/1113215	
SSBK11477_31239	CCT363294-01	BRAF	100	>10000	1.06	0.6332	1.52	-10	-14	Pass	Pass	Pass	0.76	PV3848/1113215	
SSBK11477_31239	CCT363294-01	BRAF	100	>10000	1.06	0.6332	0.508	9	-6	Pass	Pass	Pass	0.76	PV3848/1113215	

For the screening protocol and assay conditions see: https://www.thermofisher.com/uk/en/home/life-science/drug-discovery/target-and-lead-identification-and-validation/kinasebiology/kinase-activity-assays/z-lyte.html

BRAF: [ATP]=100 µM Cascade

The 2X BRAF/inactive MAP2K1 (MEK1)/inactive MAPK1 (ERK2)/Ser/Thr 03 mixture is prepared in 50 mM HEPES pH 7.5, 0.01 % BRIJ-35, 10 mM $MgCl_2$, 1 mM EGTA. The final 10 µL kinase reaction consists of 0.03-0.1 ng BRAF, 1X inactive MAP2K1 (MEK1)/inactive MAPK1 (ERK2), and 2 µM Ser/Thr 03 in 50 mM HEPES pH 7.5, 0.01 % BRIJ-35, 10 mM $MgCl_2$, 1 mM EGTA. After the 1 hour kinase reaction incubation, 5 µL of a 1:1024 dilution of development reagent A is added.

Kinase Panel Data

http://www.kinase-screen.mrc.ac.uk/services/premier-screen, accessed April 2017.

The principal method utilized is a radioactive filter binding assay using ^{33}P ATP (*Hastie, et al 2006. Nat Protoc. 2006;1(2):968-71; Bain, et al 2007. Biochem J. 2007 Dec 15;408(3):297-315*). This method is sensitive, accurate and provides a direct measure of activity.

Assay step-by-step process:

1. Upon receipt of your small molecule, staff at the ICKP will dilute each to the appropriate concentration (if required)
2. This compound is added to a 'mother plate' consisting of customer samples, controls and blanks
    - These serve as the source for 'daughter plates' which are stored at -20* until assay initiation
    - Note: All compounds are screened in duplicate
3. Next there will be 3 additions to the assay:
    - Enzyme-substrate mixture

- Incubation Time: 5 minutes at Room Temperature (RT)
- ^{33}P ATP - Assay begins with this addition
  - Incubation time varies based upon optimal designated incubation time(for each enzyme @ RT
- Orthophosphoric acid - Assay is halted with this addition

4. Assay components are harvested onto P81 filter plate
5. Filter plates are air-dried
6. Scintillation fluid is added to plates
7. Counts are read on a Topcount NXT

Data Analysis:

1. Bar codes assigned to each file ensure that data corresponding to the correct compound is being analysed
2. After completion of each assay, ICKP staff ensure that the run has passed standard quality control measures by examining reference compounds on the QC plate
3. Upon determination that the run has met QC standards, a Z-Prime (Z') value is calculated utilizing data from the controls/blanks on each individual plate
   - This QC measure is in place to ensure that *each individual plate* in the run has passed QC
4. Finally, a mean percentage activity is calculated for for each customer.
   - A standard deviation for all the duplicates is also calculated

Table S4. Aminopyrimidine 1 TAOK1 Screening Data

	10	3	1	0.3	0.1	0.03	0.01	0.003	0.001	0.0003	11	12
CCT250006	1838	3530	8016	11703	15342	*21403*	23344	20166	19257	19795	19623	*102*
CCT250006	2268	3974	9138	13921	15055	18963	19597	20704	15969	20081	17286	120

control	18454.5	AVR =	0.272
blank	111		
c-b	18343.5		

Conc.(μM)	Conc.(nM)	LOG Conc	CCT250006	CCT250006	mean	s.d.
0.0003	0.3	-0.522879	107	109	108	1
0.001	1	0.000000	104	86	95	13
0.003	3	0.477121	109	112	111	2
0.01	10	1.000000	127	106	116	14
0.03	30	1.477121	116	103	109	9
0.1	100	2.000000	83	81	82	1
0.3	300	2.477121	63	75	69	9
1	1000	3.000000	43	49	46	4
3	3000	3.477121	19	21	20	2
10	10000	4.000000	9	12	11	2
					494.4	
		IC50(μM)			**0.49**	

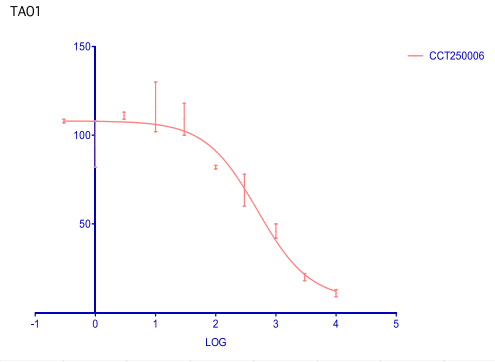

Table S5. Aminopyrimidine 1 HIPK2 Screening Data

conc.(μM)	10	3	1	0.3	0.1	0.03	0.01	0.003	0.001	0.0003	control	blank
CCT250006	182	248	963	1384	4113	6756	13461	14923	14757	15522	15972	46
CCT250006	835	616	870	1828	5503	6204	13757	18904	16749	14823	15254	44
	52	58	66	76	54	46	54	89	70	54	13224	56
	40	60	85	82	50	66	54	87	38	62	16624	52
	70	85	76	78	52	83	66	46	84	56	16513	35
	130	85	76	76	71	110	93	77	56	89	15277	39
	52	85	79	68	58	107	58	60	56	177	15490	32
	79	62	161	43	79	79	46	212	62	62	16996	39

control	15668.75	AVR =	0.229
blank	42.875		
c-b	15625.88		

Conc.(μM)	Conc.(nM)	LOG Conc	CCT250006	CCT250006
0.0003	0.3	-0.522879	99	95
0.001	1	0.000000	94	107
0.003	3	0.477121	95	121
0.01	10	1.000000	86	88
0.03	30	1.477121	43	39
0.1	100	2.000000	26	35
0.3	300	2.477121	9	11
1	1000	3.000000	6	5
3	3000	3.477121	1	4
10	10000	4.000000	1	5
			30.4	27.16
		IC50(μM)	**0.03**	**0.03**

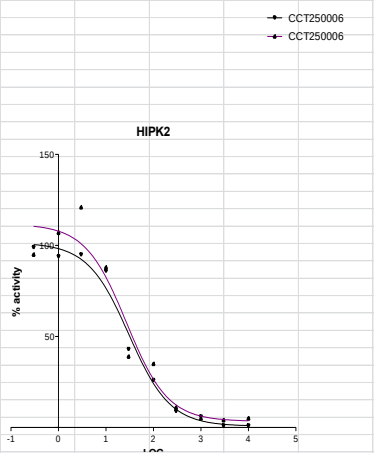

Crystallography Experimental

Protein production, purification and crystallogenesis;

Full-length 6His-tagged Pirin was produced in *E.coli* and purified as previously described.(1) Purified Pirin was crystallized in the apo form at 4 °C using the hanging-drop vapor-diffusion method. The crystallization drops were composed of 1 µL of protein (50 mg/mL) and 1 µL of reservoir solution containing 0.1 M HEPES (pH 7.5), 8 % ethylene glycol, 20 % (w/v) PEG 8,000, placed over 200 µL of reservoir solution. Needle-shaped crystals typically grew in two weeks. Pirin ligand complexes were formed by soaking apo crystals for 48 h in 25 mM of ligand in matching reservoir condition, and 20 % (v/v) DMSO. Soaked protein crystals were then briefly transferred to cryoprotectant solution of 0.1 M HEPES (pH 7.5), 8 % ethylene glycol, 22 % (w/v) PEG 8,000, 20 % Glycerol and cryocooled to 100 K in liquid nitrogen prior to data collection.

(1) Zeng, Q.; Li, X.; Bartlam, M.; Wang, G.; Pang, H.; Rao, Z. Purification, crystallization and preliminary x-ray analysis of human pirin. Acta Crystallogr., Sect. D: Struct. Biol. 2003, 59, 1496−1498.

Data collection, processing and refinement:

X-ray data were collected at the European Synchrotron Radiation Facility (ESRF) on beam-lines ID30A-1/MASSIF-1 and ID23-2. Crystals belonged to the space group $P2_12_12_1$ and diffracted to a resolution between 1.54 and 1.69 Å. Datasets were integrated with XDS (1) and scaled and merged with AIMLESS (2). Structures were solved by molecular replacement using PHASER (3, 4) with a publicly available Pirin structure (PDB codes 5JCT) with ligand and water molecules removed used as molecular replacement model. The protein−ligand structure was manually corrected and rebuilt in COOT (5) and refined with BUSTER (6) in iterative cycles. Ligand restraints were generated with GRADE (7) and MOGUL (8). The quality of the structures was assessed with MOLPROBITY (9, 10).

(1) Kabsch, W. Xds. *Acta Crystallogr., Sect. D* **2010**, *66*, 125−132.

(2) Evans, P. Scaling and Assessment of Data Quality. *Acta Crystallogr., Sect. D* **2006**, *62*, 72−82.

(3) McCoy, A. J.; Grosse-Kunstleve, R. W.; Adams, P. D.; Winn, M. D.; Storoni, L. C.; Read, R. J. Phaser Crystallographic Software. *J. Appl. Crystallogr.* **2007**, *40*, 658−674

(4) Winn, M. D.; Ballard, C. C.; Cowtan, K. D.; Dodson, E. J.; Emsley, P.; Evans, P. R.; Keegan, R. M.; Krissinel, E. B.; Leslie, A. G.; McCoy, A.; McNicholas, S. J.; Murshudov, G. N.; Pannu, N. S.; Potterton, E. A.; Powell, H. R.; Read, R. J.; Vagin, A.; Wilson, K. S. Overview of the CCP4 Suite and Current Developments. *Acta Crystallogr., Sect. D* **2011**, *67*, 235−242.

(5) Emsley, P.; Cowtan, K. Coot: Model-building Tools for Molecular Graphics. *Acta Crystallogr., Sect. D* **2004**, *60*, 2126−2132.

(6) Bricogne, G.; Blanc, E.; Brandl, M.; Flensburg, C.; Keller, P.; Paciorek, W.; Roversi, P.; Sharff, A.; Smart, O. S.; Vonrhein, C.; Womack, T. O. *BUSTER*, version 2.10.2; Global Phasing Ltd.: Cambridge, United Kingdom, **2015**.

(7) Smart, O. S.; Womack, T. O.; Sharff, A.; Flensburg, C.; Keller, P.; Paciorek, W.; Vonrhein, C.; Bricogne, G. *Grade*, version 1.2.9; Global Phasing Ltd.: Cambridge, United Kingdom, **2014**.

(8) Bruno, I. J.; Cole, J. C.; Lommerse, R. S.; Rowland, R.; Taylor, R.; Verdonk, M. L. Isostar: A Library of Information About Non-bonded Interactions. *J. Comput.-Aided. Mol. Des.* **1997**, *11*, 525−537.

(9) Chen, V. B.; Arendall III, W. B.; Headd, J. J.; Keedy, D. A.; Immormino, R. M.; Kapral, G. J.; Murray, L. W.; Richardson, J. S.; Richardson, D. C. MolProbity: All-atom Structure Validation for Macromolecular Crystallography. *Acta Crystallogr., Sect. D* **2010**, *66*, 12−21.

(10) Davis, I. W.; Leaver-Fay, A.; Chen, V. B.; Block, J. N.; Kapral, G. J.; Wang, X.; Murray, L. W.; Arendall, W. B., 3rd; Snoeyink, J.; Richardson, J. S.; Richardson, D. C. MolProbity: All-atom Contacts and Structure Validation for Proteins and Nucleic Acids. *Nucleic Acids Res.* **2007**, *35*, W375−W383.

Table S6: Crystallographic data collection and refinement statistics:

Protein construct	Pirin 1-290	Pirin 1-290
Ligand	**2**	**7**
PDB code	6H1I	6H1H
Crystal		
Space group	P 2_1 2_1 2_1	P 2_1 2_1 2_1
Unit cell dimensions (a/b/c in Å)	42.05/67.15/107.24	42.30/67.41/107.68
Unit cell angles (α/β/γ in °)	90/90/90	90/90/90
Data collection and processing		
Beamline	ESRF ID30A-1	ESRF ID23-2
Wavelength (Å)	0.9650	0.8726
Integration program	XDS	XDS
Reduction program	AIMLESS	AIMLESS
Resolution range	41.90 – 1.69	42.30 – 1.54
Number of unique reflections [a]	33746 (1702)	46420 (2277)
Completeness [a]	97.3 (98.4)	99.8 (99.6)
Redundancy [a]	4.3 (4.5)	6.5 (6.4)
R_{merge} (%) [a]	12 (144.6)	10.5 (136.7)
I/σ(I) [a]	7.7 (1.2)	10.1 (1.3)
$CC_{1/2}$ [a, b]	0.986 (0.375)	0.998 (0.344)
Refinement		
Program	BUSTER	BUSTER
R_{work} (%)	17.87	15.86
R_{free} (%)	22.42	18.29
Number of residues	287	288
Number of water molecules	272	349
Average B-factor (Å^2)	25.73	24.76
Ramachandran favoured (%)	97.54	97.55
Ramachandran outliers (%)	0	0
RMSD bonds (Å)	0.014	0.014
RMSD angles (°)	1.75	1.66

[a] Values in parentheses are for the highest resolution shell.

[b] Half-dataset correlation coefficient, see: Karplus, P. A.; Diederichs, K. Linking crystallographic model and data quality. *Science* **2012**, *336*, 1030−1033.

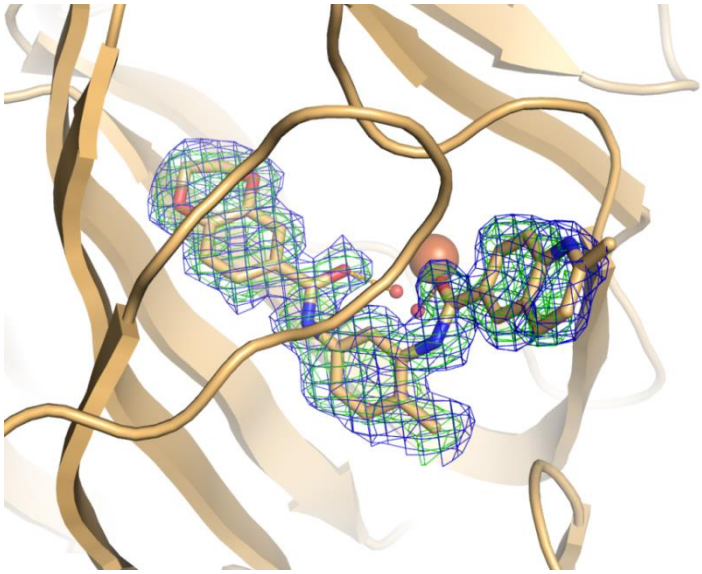

Figure S15. Structure of Bisamide 2 bound to Pirin, with final 2Fo-Fc map contoured at 1 σ shown as blue mesh, and omit Fo-Fc map contoured at 3 σ shown as green mesh.

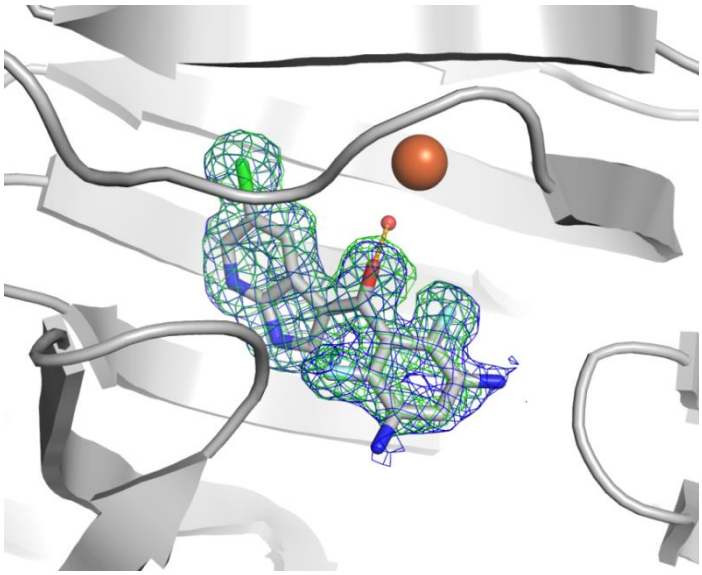

Figure S16. Structure of PLX4720 7 bound to Pirin, with final 2Fo-Fc map contoured at 1 σ shown as blue mesh, and omit Fo-Fc map contoured at 3 σ shown as green mesh.